Inorganic AlCl₃−alkali metal thiocyanate ionic liquids as electrolytes for electrochemical Al technologies

SCHOLARONE™
Manuscripts

Chemical Communications

Inorganic AlCl₃–alkali metal thiocyanate ionic liquids as electrolytes for electrochemical Al technologies

Chih-Yao Chen,[a,b] Tetsuya Tsuda[*a] and Susumu Kuwabata[*a]

A series of inorganic AlCl₃–alkali metal thiocyanate (A$_M$SCN: A$_M$ = Li, Na, K) ionic liquids (ILs) is demonstrated as electrolytes for Al electrodeposition and Al-anion rechargeable batteries (AARBs) at 303–363 K. Al deposits with a unique flake nanostructure are obtained in these electrolytes. The assembled AARBs show a stable cyclability over 250 cycles with a reversible capacity of ca. 70 mAh (g-graphite)$^{-1}$ at 363 K. These inorganic ILs inherit the advantages of conventional chloroaluminate ILs (applicability at near-ambient temperature) and molten salts (cost effectiveness), making them promising electrolyte candidates for industrializable electrochemical Al technologies.

Ionic liquids (ILs), which are liquids composed entirely of ions and have melting points below 373 K, have attracted growing academic and industrial interests for diverse technologies over the past decades.[1,2] Owing to their remarkable electrochemical stability, ILs have been considered as an ideal platform for electrodeposition of a variety of technologically important and electropositive elements.[3–6] Through manipulating the cation and anion combination, ILs are expected to provide unprecedented approach to not only control the nucleation process and the morphology of the deposit but also stabilize nanosized deposits.[7,8] The aluminum (Al) electrodeposition using ILs has a venerable history.[9,10] Research in this realm has regained attention owing to recent advancements of Al-anion rechargeable batteries (AARBs), whose rechargeability strongly depends on the reversibility of Al metal anodes.[11–13] Typical electrolytes for these studies are Lewis acidic chloroaluminate ILs composed of AlCl₃ and organic salts such as 1-ethyl-3-methylimidazolium chloride ([C₂mim]Cl) and 1-(1-butyl)pyridinium chloride. However, these organic salts are costly and not easy to prepare. These drawbacks limit the industrial-scale application of IL-based Al electrodeposition and lessen the economic benefits anticipated for Al secondary batteries.[14–16] Despite the fact that some electrolytes have been identified as inexpensive alternatives,[17–20] none of them supports facile Al deposition and stripping as chloroaluminate ILs.

Inorganic chloroaluminate molten salts based on AlCl₃ and alkali metal chloride(s) are promising candidates within this context.[21,22] They are not only capable of supporting reversible Al deposition–stripping but also readily available at a reasonable cost (e.g., 9.7 USD kg^{-1} for AlCl₃–NaCl versus 71.3 USD kg^{-1} for AlCl₃–[C₂mim]Cl).[23] Furthermore, the greater packing efficiency of constituent ions and high concentration of Al species (e.g., 6.0 M AlCl₃–NaCl versus 3.4 M for AlCl₃–[C₂mim]Cl)[24] resulted from the exclusion of bulky organic cations are also beneficial for the cell-level energy density of AARBs.[25] Nonetheless, inorganic chloroaluminates generally require a liquidus temperature above 373 K,[26] which inevitably restricts their use to specific applications.[27–29]

Pseudohalides (CN$^-$ and XCN$^-$, X = O, S, Se) are polyatomic groups that have similar physicochemical properties and coordination ability to halides. They can fine-tune the electronic structure and steric effect of several metal complexes that are otherwise impossible by solely halide ions. In particular, thiocyanates (SCN$^-$) have been adopted to substitute the halide ligand in synthesizing new ILs of low melting points due to the low symmetry and charge delocalization of SCN$^-$ anions.[30–32] In this study, we show that the replacement of alkali metal halide(s) with their thiocyanate counterpart(s) in inorganic chloroaluminates could effectively decrease the melting temperature and help to retain the liquid nature at near-ambient temperature. These electrolytes enable Al deposition over an easy-to-use temperature range of 303–363 K and allow AARB to function over 333–363 K. The present study would pave the way towards the development of inorganic ILs with both cost effectiveness and desired (electro)chemical properties.

Fig. 1a shows differential scanning calorimetry (DSC) results for a series of AlCl₃–A$_M$SCN (A$_M$ = Li, Na, K) in selected

[a] Department of Applied Chemistry, Graduate School of Engineering, Osaka University, 2-1 Yamada-oka, Suita, Osaka 565-0871, Japan. E-mail: ttsuda@chem.eng.osaka-u.ac.jp or kuwabata@chem.eng.osaka-u.ac.jp
[b] AIST-Kyoto University Chemical Energy Materials Open Innovation Laboratory (ChEM-OIL), National Institute of Advanced Industrial Science and Technology (AIST), Sakyo-ku, Kyoto 606-8501, Japan
† Electronic Supplementary Information (ESI) available. See DOI: 10.1039/x0xx00000x
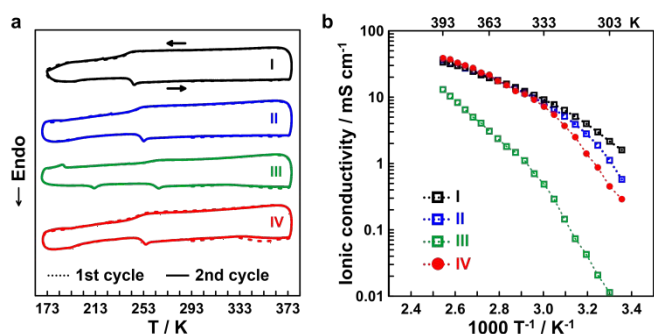
Fig. 1 (a) DSC thermograms of (I) AlCl$_3$–LiSCN (67 : 33 mol%), (II) AlCl$_3$–NaSCN (67 : 33 mol%), (III) AlCl$_3$–KSCN (67 : 33 mol%), and (IV) AlCl$_3$–NaSCN–KSCN (61 : 26 : 13 mol%) measured at a heating/cooling rate of 5 K min^{-1}. (b) Ionic conductivity of AlCl$_3$–A$_M$SCN melts over 298–393 K.

molar ratios at which inorganic chloroaluminate molten salts generally exhibit the lowest melting point.[26,28] For the binary mixtures, the glass transition temperature (T_g) is found to increase with increasing alkali metal cation size, which is observed at ca. 245, 253, and 266 K for AlCl$_3$–LiSCN (67 : 33 mol%), AlCl$_3$–NaSCN (67 : 33 mol%), and AlCl$_3$–KSCN (67 : 33 mol%), respectively. For the ternary mixture AlCl$_3$–NaSCN–KSCN (61 : 26 : 13 mol%), the T_g is discernible at about 255 K. Notably, T_g of these electrolytes are much lower than most inorganic binary salts reported (e.g., 300 K for AlCl$_3$–NaN(CN)$_2$ (50 : 50 mol%), 287 K for AlCl$_3$–ZnCl$_2$ (40 : 60 mol%)).[33,34] Furthermore, the melting temperature of all AlCl$_3$–A$_M$SCN systems is visually confirmed at ca. 323–338 K, which is considerably lower as compared to AlCl$_3$–A$_M$Cl analogues (380–416 K).[26] It is supposed that the formation of large complex anions, [Al$_n$Cl$_{3n-m+1}$(SCN)$_m$]$^-$,[35] weakens the coulomb interactions between ions, resulting in the apparent depression in melting points. It is worth noting that AlCl$_3$–A$_M$SCN melts show a strong tendency to form supercooled liquids upon cooling and exhibit a certain fluidity after storage at room temperature for an extended period. The easy formation of supercooled states may originate from the ambidentate character of thiocyanate anions that complicates the solution structure and makes crystallization difficult.[36] This property is advantageous as applied to electrochemical devices because it allows the fluid interfacial contact between the electrode and electrolyte to be maintained even at the temperature below the melting point of the electrolytes.

Fig. 1b presents the ionic conductivity of AlCl$_3$–A$_M$SCN over the temperature range from 298 to 393 K. As can be seen, the conductivity increases with increasing temperature, and the downward curve of these data plots is recognized. The ionic conductivity is 1.60, 0.58, and 0.29 mS cm^{-1} at 298 K for AlCl$_3$–LiSCN, AlCl$_3$–NaSCN, and AlCl$_3$–NaSCN–KSCN, respectively. The conductivity reaches approximately 10 mS cm^{-1} at 333 K, with the exception of AlCl$_3$–KSCN. As shown in Fig. S1 (ESI†), the viscosity of these melts shows the upward curve as a function of temperature. The change of the slope of Arrhenius plots observed for all ILs implies these ILs have different activation energies for ion transport controlled by liquid structure. The non-Arrhenius temperature dependences obtained

from the conductivity and the viscosity are in consistent with most glass-forming liquids.[36]

Fig. 2 shows the cyclic voltammograms (CV) of Al deposition–stripping in AlCl$_3$–A$_M$SCN melts with a Pt working electrode at 333 K. The cathodic current corresponding to the Al deposition rises steeply at a potential of ca. –0.5 V. The cathodic current density of these melts at –0.75 V follows the order, AlCl$_3$–LiSCN > AlCl$_3$–NaSCN–KSCN > AlCl$_3$–NaSCN > AlCl$_3$–KSCN. A current loop is observed in the reverse scan in some cases, indicating the deposition is predominately governed by nucleation.[37] Similar behavior has been reported in the Lewis acidic chloroaluminate ILs.[37,38] Although certain overpotential is required for Al nucleation, the anodic peak occurs at ca. 0.0 V, suggesting the acceptably good reversibility of Al deposition–stripping in these melts. Interestingly, CV profiles measured in the supercooled melts at 303 K are generally similar to those at 333 K, showing their potential ambient-temperature applicability (Fig. S2, ESI†). Besides, it comes as no surprise that the cathodic and anodic current remarkably increase and the reduction onset potential shifts to less negative potential at 363 K, indicating enhanced electrode kinetics at elevated temperatures as a result of decreased viscosity and facilitated transport of electroactive species toward the electrode (Fig. S3, ESI†).[21] Based on above results, the operational temperature range for the AlCl$_3$–A$_M$SCN electrolytes is verified to be 303–393 K, which is attractively low.

Whereas the metallic Al layer is commonly electrodeposited in haloaluminate ILs,[10] the visual appearance of Al deposits obtained in AlCl$_3$–A$_M$SCN is nearly black. This could be
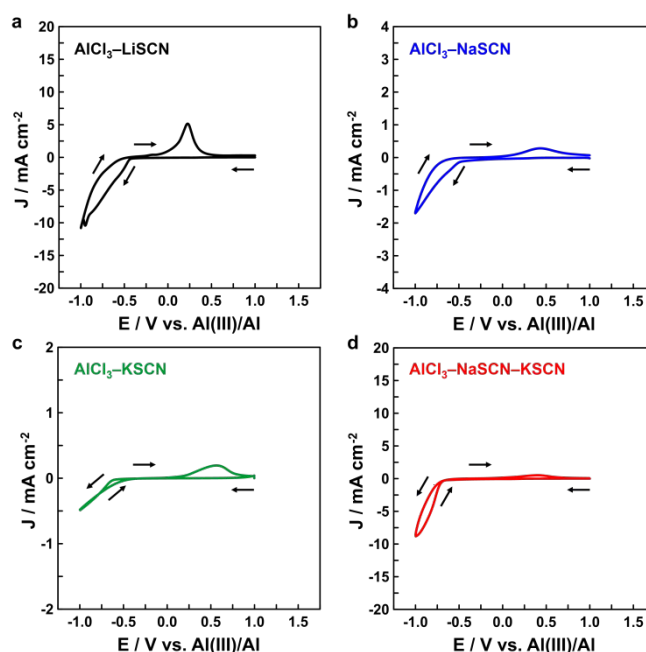
Fig. 2 Cyclic voltammograms of Al deposition–stripping in (a) AlCl$_3$–LiSCN (67 : 33 mol%), (b) AlCl$_3$–NaSCN (67 : 33 mol%), and (c) AlCl$_3$–NaSCN–KSCN (61 : 26 : 13 mol%) in a three-electrode cell using a Pt wire as the working electrode and Al wires as the reference and counter electrodes. The scan rate was 10 mV s^{-1}. The temperature was 333 K. Note that different scales have been used for each voltammogram for clarity.
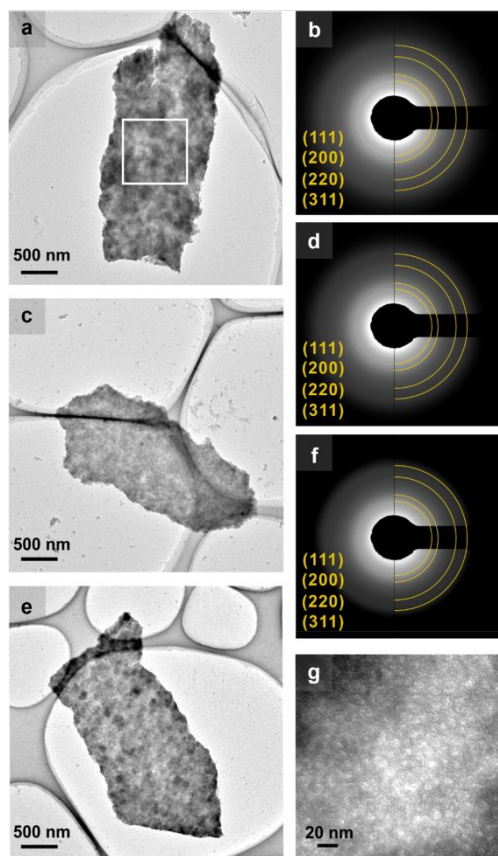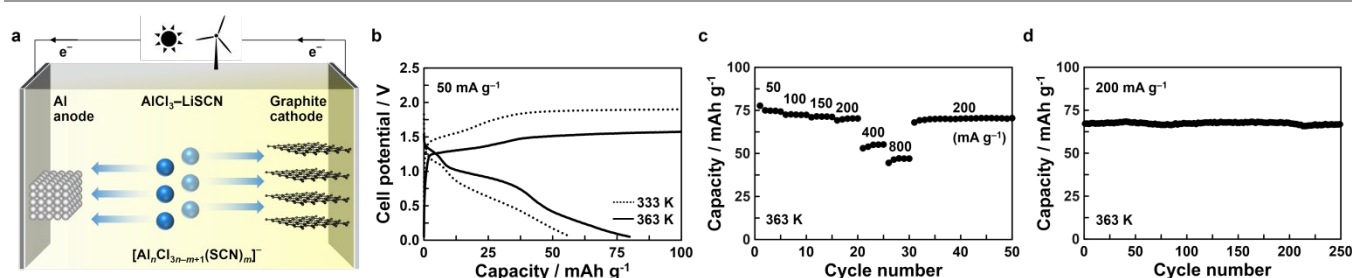
Fig. 3 TEM micrographs and corresponding selected area electron diffraction (SAED) patterns of Al deposits obtained by potentiostat deposition at −0.70 V (vs. Al(III)/Al) at 333 K for 30 min in (a, b) AlCl₃–LiSCN (67 : 33 mol%), (c, d) AlCl₃–NaSCN (67 : 33 mol%), and (e, f) AlCl₃–NaSCN–KSCN (61 : 26 : 13 mol%). (g) High-resolution TEM image of the area marked by the white square in (a).

indicate these deposits are face-centered cubic Al (PDF 00-004-0787), while the diffused ring patterns suggest the crystallinity is low. This peculiar morphology of Al deposits may contribute to the favorable stripping shown in Fig. 2.

Al electroplating has been intensively investigated for corrosion protection purpose, while fabrication of Al with a controlled nanostructure through electrochemical methods is scarcely reported.[39,40] According to these studies, the morphology of Al deposits can be greatly influenced by electrolyte speciation and electrodeposition parameters. As compared to Lewis acidic $AlCl_3$–A_MCl in which $[Al_nCl_{3n+1}]^-$ is the dominant species, the less mobile and lower symmetry features of $[Al_nCl_{3n-m+1}(SCN)_m]^-$ in $AlCl_3$–A_MSCN and more complex by-product chemical species generated during the Al deposition process possibly restrict the free Al growth and cause the formation of low-dimensional nanosized Al. However, because the speciation equilibrium of $AlCl_3$–A_MSCN systems remains largely unknown, it is difficult to propose even the possible mechanism at this stage.

Despite the fact that AARBs have been considered as the emerging energy storage technologies, only few efforts have been made to improve their performance by modifying the electrolyte.[15,16,27–29] So far, most studies on alternative Al complex anion-conducting electrolytes have focused almost exclusively on their physicochemical properties and Al plating aspects, while their feasibility as battery electrolytes have rarely been assessed. In order to evaluate the applicability of $AlCl_3$–A_MSCN inorganic ILs as electrolytes for AARB application, a graphite sheet was used as the cathode active material coupled with an Al plate as the anode (Fig. 4a). Among the electrolytes investigated, $AlCl_3$–LiSCN (67 : 33 mol%) shows the highest coulombic efficiency for Al deposition–stripping and therefore appears to be the preferred candidate. Fig. 4b displays typical charge-discharge curves of the Al | $AlCl_3$–LiSCN | graphite cell. A discharge capacity of 57 mAh g⁻¹ at 50 mA g⁻¹ is obtained at 333 K but with a large voltage hysteresis that is most likely caused by the overpotential required for Al deposition as discussed above.[41] At 363 K, the voltage hysteresis remarkably decreases and the discharge plateaus becomes more unambiguous. Consequently, the reversible capacity is enhanced to 80 mAh g⁻¹. The rate performance of the cell indicates that 88%, 69%, and 59% of the capacity could be maintained at a current density of 200, 400, and 800 mA g⁻¹, respectively (Fig.

originated from the fine size and large specific surface area of the deposits.[38] Fig. 3 and Fig. S4 (ESI†) show representative TEM micrographs and the corresponding selected area electron diffraction (SAED) patterns of the deposits acquired at 333 K at −0.70 V for 30 min. It can be seen that the deposits exhibit a two-dimensionally flake-like structure with a width of several micrometers, irrespective of the IL electrolytes used. The porous feature and ultrathin thickness of these deposits can be ascertained from the high-resolution images (Fig. 3g) and from their electron transparency as the underlying lacey formvar/carbon support is clearly discernible. SAED patterns

Fig. 4 (a) Schematic illustration of an AARB constructed with Al as the anode, graphite as the cathode, and AlCl₃–LiSCN (67 : 33 mol%) as the electrolyte. (b) Galvanostatic charge-discharge curves measured at a current density of 50 mA g⁻¹ at 333 (dotted line) and 363 K (solid line). Cycling performance of the Al | AlCl₃–LiSCN | graphite cell (c) at various rates ranging from 50 to 800 mA g⁻¹ and (d) at 200 mA g⁻¹ recorded at 363 K.

4c and S5a in ESI†). Importantly, no obvious capacity fade is observed after 250 cycles, confirming the stability of both the electrolyte and the cathode (Fig. 4d and S5b in ESI†). Assembling the cell with other inorganic melts was also attempted. The electrochemical properties are not as good as those tested in the AlCl$_3$–LiSCN under the same condition (Fig. S6). Nevertheless, we are confident that the development of affordable inorganic IL electrolytes like AlCl$_3$–A$_M$SCN could promote Al-based batteries as practically viable energy storage systems. Being free of bulky cation organic salts, the high ionic concentration of inorganic electrolytes is also expected to boost the weight-specific performance.

In summary, the electrochemical behavior of Al deposition–stripping has been investigated in a series of AlCl$_3$–A$_M$SCN over 303–363 K. The novelty of these electrolytes lies in being a completely inorganic system but exhibits a melting point within the range commonly observed for organic salt-based ILs. AARBs utilizing AlCl$_3$–LiSCN electrolytes exhibit good reversible capacity and cyclability at 363 K. The utilization of pseudohalide salts can therefore be considered as a promising strategy to develop cost-effective and low-melting AlCl$_3$-based IL electrolytes.

Conflicts of interest

There are no conflicts to declare.

Notes and references

1   M. Watanabe, M. L. Thomas, S. G. Zhang, K. Ueno, T. Yasuda and K. Dokko, *Chem. Rev.*, 2017, **117**, 7190.
2   X. P. Zhang, X. C. Zhang, H. F. Dong, Z. J. Zhao, S. J. Zhang and Y. Huang, *Energy Environ. Sci.*, 2012, **5**, 6668.
3   F. Endres, M. Bukowski, R. Hempelmann and H. Natter, *Angew. Chem. Int. Ed.*, 2003, **42**, 3428.
4   M. J. Deng, P. Y. Chen, T. I. Leong, I. W. Sun, J. K. Chang and W. T. Tsai, *Electrochem. Commun.*, 2008, **10**, 213.
5   S. Murugesan, O. A. Quintero, B. P. Chou, P. H. Xiao, K. Park, J. W. Hall, R. A. Jones, G. Henkelman, J. B. Goodenough and K. J. Stevenson, *J. Mater. Chem. A*, 2014, **2**, 2194.
6   A. P. Abbott and K. J. Mckenzie, *Phys. Chem. Chem. Phys.*, 2006, **8**, 4265.
7   M. Armand, F. Endres, D. R. MacFarlane, H. Ohno and B. Scrosati, *Nat. Mater.*, 2009, **8**, 621.
8   S. F. L. Mertens, C. Vollmer, A. Held, M. H. Aguirre, M. Walter, C. Janiak and T. Wandlowski, *Angew. Chem. Int. Ed.*, 2011, **50**, 9735.
9   Y. G. Zhao and T. J. VanderNoot, *Electrochim. Acta*, 1997, **42**, 3.
10 T. Tsuda, G. R. Stafford and C. L. Hussey, *J. Electrochem. Soc.*, 2017, **164**, H5007.
11 M. C. Lin, M. Gong, B. G. Lu, Y. P. Wu, D. Y. Wang, M. Y. Guan, M. Angell, C. X. Chen, J. Yang, B. J. Hwang and H. J. Dai, *Nature*, 2015, **520**, 324.
12 H. Chen, H. Y. Xu, S. Y. Wang, T. Q. Huang, J. B. Xi, S. Y. Cai, F. Guo, Z. Xu, W. W. Gao and C. Gao, *Sci. Adv.*, 2017, **3**, eaao7233.
13 X. W. Yu and A. Manthiram, *Adv. Energy Mater.*, 2017, **7**, 1700561.
14 C. K. Zhang, Y. Ding, L. Y. Zhang, X. L. Wang, Y. Zhao, X. H. Zhang and G. H. Yu, *Angew. Chem. Int. Ed.*, 2017, **56**, 7454.
15 M. Angell, C. J. Pan, Y. M. Rong, C. Z. Yuan, M. C. Lin, B. J. Hwang and H. J. Dai, Proc. Natl. Acad. Sci. USA, 2017, **114**, 834.
16 C. Li, J. Patra, J. Li, P. C. Rath, M. H. Lin and J. K. Chang, *Adv. Funct. Mater.*, 2020, **30**, 1909565.
17 T. Mandai and P. Johansson, *J. Mater. Chem. A*, 2015, **3**, 12230.
18 A. Kitada, K. Nakamura, K. Fukami and K. Murase, *Electrochim. Acta*, 2016, **211**, 561.
19 Y. X. Fang, K. Yoshii, X. G. Jiang, X. G. Sun, T. Tsuda, N. Mehio and S. Dai, *Electrochim. Acta*, 2015, **160**, 82.
20 Y. Nakayama, Y. Senda, H. Kawasaki, N. Koshitani, S. Hosoi, Y. Kudo, H. Morioka and M. Nagamine, *Phys. Chem. Chem. Phys.*, 2015, **17**, 5758.
21 J. S. Wilkes, *Green Chem.*, 2002, **4**, 73.
22 M. Ueda, *J. Solid State Electrochem.*, 2017, **21**, 641.
23 K. V. Kravchyk and M. V. Kovalenko, *Commun. Chem.*, 2020, **3**, 120.
24 L. Xiao, J. S. Wilkes and K. E. Johnson, *Proceedings of the 13th International Symposium on Molten Salts*, 2002, **2002-19**, 964.
25 K. V. Kravchyk, C. Seno and M. V. Kovalenko, *ACS Energy Lett.*, 2020, **5**, 545.
26 G. J. Janz, R. P. T. Tomkins, C. B. Allen, J. R. Downey, G. L. Garner, U. Krebs and S. K. Singer, *J. Phys. Chem. Ref. Data*, 1975, **4**, 871.
27 Y. Song, S. Q. Jiao, J. G. Tu, J. X. Wang, Y. J. Liu, H. D. Jiao, X. H. Mao, Z. C. Guo and D. J. Fray, *J. Mater. Chem. A*, 2017, **5**, 1282.
28 C. Y. Chen, T. Tsuda, S. Kuwabata and C. L. Hussey, *Chem. Commun.*, 2018, **54**, 4164.
29 J. Wang, X. Zhang, W. Q. Chu, S. Q. Liu and H. J. Yu, *Chem. Commun.*, 2019, **55**, 2138.
30 T. Peppel, M. Kockerling, M. Geppert-Rybczynska, R. V. Ralys, J. K. Lehmann, S. P. Verevkin and A. Heintz, *Angew. Chem. Int. Ed.*, 2010, **49**, 7116.
31 P. Nockemann, B. Thijs, N. Postelmans, K. Van Hecke, L. Van Meervelt and K. Binnemans, *J. Am. Chem. Soc.*, 2006, **128**, 13658.
32 C. L. Liu and C. A. Angell, *Solid State Ionics*, 1996, **86–88**, 467.
33 Y. C. Lee, L. A. Curtiss, M. A. Ratner and D. F. Shriver, *Chem. Mater.*, 2000, **12**, 1634.
34 S. Pedersen, *Viscosity, Structure and Glass Formation in the AlCl$_3$–ZnCl$_2$ system*, Fakultet for Naturvitenskap Og Teknologi, 2001.
35 C. L. Liu, D. Teeters, W. Potter, B. Tapp and M. H. Sukkar, *Solid State Ionics*, 1996, **86–88**, 431.
36 P. G. Debenedetti and F. H. Stillinger, *Nature*, 2001, **410**, 259.
37 S. Z. E. Abedin, P. Giridhar, P. Schwab and F. Endres, *Electrochem. Commun.*, 2010, **12**, 1084.
38 A. P. Abbott, F. Qiu, H. M. A. Abood, M. R. Ali and K. S. Ryder, *Phys. Chem. Chem. Phys.*, 2010, **12**, 1862.
39 E. Perre, L. Nyholm, T. Gustafsson, P. L. Taberna, P. Simon and K. Edstrom, *Electrochem. Commun.*, 2008, **10**, 1467.
40 C. J. Su, Y. T. Hsieh, C. C. Chen and I. W. Sun, *Electrochem. Commun.*, 2013, **34**, 170.
41 H. J. Tian, S. L. Zhang, Z. Meng, W. He and W. Q. Han, *ACS Energy Lett.*, 2017, **2**, 1170.

Table of Contents

Inorganic ionic liquids, $AlCl_3–A_MSCN$ (A_M = Li, Na, K), were developed and found to support Al deposition and Al-anion rechargeable batteries over an easy-to-use temperature range of 303–363 K.